Article

Cargo Transport at Microtubule Crossings: Evidence for Prolonged Tug-of-War between Kinesin Motors

Olaolu Osunbayo,[1] Jacqualine Butterfield,[1] Jared Bergman,[1] Leslie Mershon,[1] Vladimir Rodionov,[3] and Michael Vershinin[1,2,*]

[1]Department of Physics and Astronomy and [2]Center for Cell and Genome Science, University of Utah, Salt Lake City, Utah; and [3]Department of Cell Biology, University of Connecticut, Farmington, Connecticut

ABSTRACT Intracellular transport of cargos along microtubules is often complicated by the topology of the underlying filament network. The fundamental building blocks for this complex arrangement are filament intersections. The navigation of cargos across microtubule intersections remains poorly understood. Here, we demonstrate that kinesin-driven cargos are engaged in a tug-of-war at microtubule intersections. Tug-of-war events result in long pauses that can last from a few seconds to several minutes. We demonstrate that the extent of the tug-of-war and the duration of pauses change with the number of motors on the cargo and can be regulated by ionic strength. We also show that dwell times at intersections depend on the angle between crossing microtubules. Our data suggest that local microtubule geometry can regulate microtubule-based transport.

INTRODUCTION

Cargo transport along microtubules (MTs) is a logistics technology that is essential for the function and survival of eukaryotic cells. Many key aspects of MT-based logistics in cells are only now coming into focus. There is growing interest in how cargos driven by multiple motors navigate MT intersections (1–3). Such crossings are a common feature of the cytoskeleton and can potentially regulate intracellular logistics in an entirely different fashion—via network topology, as opposed to environmental or chemical regulation. In addition, MT intersections are also likely to be the loci of local chemical regulation in cells (1,4). However, relatively little is known about the processes involved in cargo travel across MT-MT junctions.

To gain insight into the behavior of organelles at MT intersections in vivo, we examined transport of melanosomes to the cell periphery (pigment dispersion) in *Xenopus* melanophores. At early stages of pigment dispersion, melanosomes move to the plus-ends of cytoplasmic MTs driven predominantly by the kinesin-2 motors (5). Time sequences of images of melanophores with fluorescently labeled MTs (6,7) showed that melanosomes often had a reduced velocity of movement or completely stopped at MT intersections (Fig. 1 *A*; Movie S1 in the Supporting Material). Furthermore, MTs often buckled when melanosomes moving along them attached to other MTs that crossed their path (Fig. 1 *A*; Movie S1). This remarkable behavior of MTs was consistent with the application of force by cargo-bound kinesin motors simultaneously interacting with adjacent MTs.

However, other interpretations were also possible because additional motors (cytoplasmic dynein and myosin V) were also bound to melanosomes (8). Although these motors are largely inactive during pigment dispersion (8), in principle, they could generate force for MT buckling. Therefore, to examine the behavior at MT intersections of cargoes transported by kinesin motors alone, we employed a purified in vitro system. We show that cargos driven by many kinesin motors can spend extensive amounts of time at MT intersections, that such events are likely associated with a tug-of-war between multiple kinesin motors on the same cargo, and that MT bending is common if the filament deformations are not otherwise restricted (e.g., by bonds to a substrate such as a glass slide).

MATERIALS AND METHODS

Data acquisition in *Xenopus* melanophores

Xenopus melanophores were cultured in 70% L15 medium supplemented with antibiotics, 10% fetal bovine serum, and 5 mg/ml of insulin at 27°C (7). To induce pigment dispersion, cells were treated with melanocyte-stimulating hormone (10^{-8} M).

For fluorescence labeling of MTs, cells were pressure injected with Cy3-labeled bovine brain tubulin (6). Injected cells were incubated for at least 1 h at 27°C to allow for the incorporation of labeled tubulin subunits into MTs.

Fluorescence images of melanophores were acquired using a Nikon Eclipse Ti (Nikon Instrucments, Melville, NY) inverted microscope equipped with a Plan apochromat ×100 1.4 NA objective lens, and an Andor iXon EM-CCD sensor (Andor Technology USA, South Windsor, CT) driven by Metamorph image acquisition and analysis software (Molecular Devices, Sunnyvale, CA). To reduce photobleaching and photodamage,

Submitted August 6, 2014, and accepted for publication February 20, 2015.

*Correspondence: vershinin@physics.utah.edu

Editor: Ram Dixit.

0006-3495/15/03/1480/4 $2.00

http://dx.doi.org/10.1016/j.bpj.2015.02.016

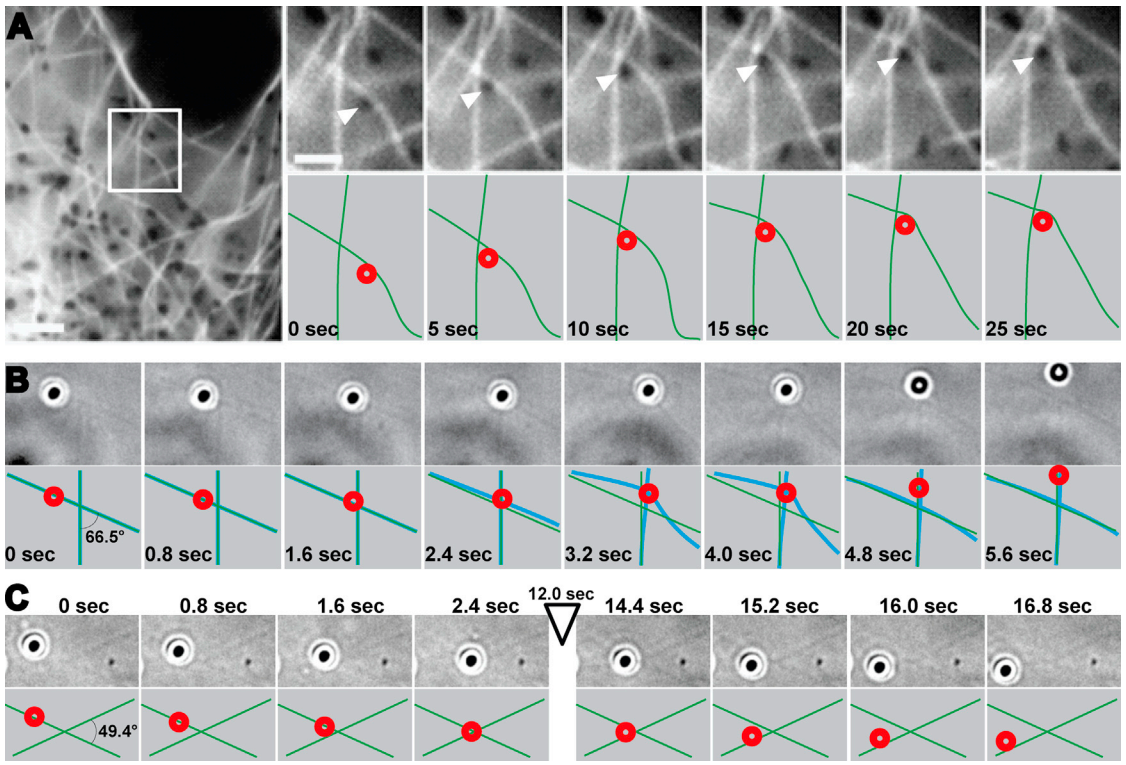

FIGURE 1 Examples of cargo dynamics at MT intersections in vivo and in vitro. (*A*) A melanosome moving along a MT in a melanophore in vivo encounters another MT that crosses its movement path. Left panel: low-magnification fluorescence image of the melanophore periphery. Right panel, top row: successive high-magnification images of the boxed images are shown in the left panel; bottom row: schematic representation of the position of the melanosome (*red circle*) and MTs (*green lines*) in the images shown in the top row. Numbers indicate time in seconds; magnification bars are 10 μm (*left panel*) and 5 μm (*right panel*). A collision of the melanosome with the crossing MT blocks its movement and leads to deformation of both crossing MTs. (*B* and *C*) Examples of cargo dynamics at MT crossings in vitro: an MT deformation event (*B*) and a very long dwell event (*C*). Numbers indicate time in seconds. Top rows: still frames of beads and MTs. Bottom rows: schematic representations of the positions of beads (*red*) and MTs (*green*) in the images shown in the top row (frame timing indicated). Blue lines show deformed geometries; fields of view: 8.5 $\times$ 4.3 μm (*B*) and 6.0 $\times$ 9.4 μm (*C*).

cells were treated with the oxygen-depleting agent Oxyrase before image acquisition.

Data acquisition in vitro

KIF5A KHC dimers were expressed in an *E. coli* system as previously described (9). Porcine tubulin was acquired from Cytoskeleton (Denver, CO) and MTs were reconstituted according to the manufacturer's protocol. Buffers and slides were prepared as previously described (1). The assay buffer was PMEE (35 mM Pipes, 5 mM $MgCl_2$, 1 mM EGTA, 0.5 mM EDTA), pH 7.2. Briefly, the flow cells were cleaned with a KOH wash, incubated with poly-L-lysine solution, and attached to a glass slide with double-sided tape. The flow chambers were assembled in a cross-flow geometry as previously described (1). Taxol-stabilized MTs were first diluted in flow buffer (assay buffer + 20 μM taxol + 1 mM GTP) and then injected into the flow cells, with a 15-min incubation after each orthogonal-direction injection. The unattached MTs were then washed away and the surface was blocked with buffer containing 20 mg/mL casein (Sigma-Aldrich, St. Louis, MO).

Carboxylated polystyrene beads (Ø1 μm or Ø3 μm; Polysciences, Philadelphia, PA) were incubated at room temperature with different concentrations of kinesin KIF5A for 15 min in the presence of dithiothreitol (2mM) and saturating ATP (2 mM ATP), and then immediately injected into the flow cells.

To achieve equivalent binding fractions in Ø1 μm and Ø3 μm bead assays, the motor concentration was increased 27-fold for the latter case. The scaling factor differs from the expected 9-fold increase in bead surface area. However, Polysciences does not produce beads with titrated concentration of carboxylic groups per bead. A similar manufacturing process used by Bangs Laboratories is known to have a wide variation of carboxyl group concentrations between bead lots (e.g., 17–207 μM carboxyl groups per 1 g of beads for Ø1 μm beads). Therefore, our ratio is well within the expected range. Due to the large variability between bead lots, we chose to use the binding fraction measurements as a direct estimate of motor activity on the beads.

Measurements were performed as previously described (10). Briefly, beads and MTs were viewed using a Nikon Eclipse Ti microscope equipped with a high-magnification, high-NA objective (Nikon Plan Apo VC 100$\times$ oil, 1.40 NA). A high-resolution camera (iXon+ DU897; Andor Technology USA, South Windsor, CT) and Nikon NIS elements AR software (Nikon Instruments, Melville, NY) were used to record experiments. Custom-built image-processing, speed-tracking, and angle-measuring software written in MATLAB (The MathWorks, Natick, MA) was used. Further analysis and curve fitting were performed with OriginPro software (OriginLab, Northampton, MA).

Most MT-MT crossing events were associated with low cargo velocities so that the beginning and the end of such dwell events could be identified from tracks of bead position for all frames. A dwell time of zero was recorded for events with no drop in cargo velocity during video records in which a cargo and both MTs visually overlapped.

Statistical tests were performed using the Wilcoxon-Mann-Whitney test. Student's *t*-test was not used, because most of the distributions tested were long tailed (not Gaussian).

RESULTS AND DISCUSSION

We used polystyrene beads with preadsorbed, recombinant, full-length dimers of heavy chains (KHC) of conventional kinesin KIF5A as model synthetic cargos. To facilitate interaction of motors with MTs, we used high surface densities of kinesin motors (Fig. S1) that significantly exceeded the densities used in previous studies (1,2). To examine MT-MT intersections for a variety of angles, we employed the crossed-flow geometry (1,2) and admitted MTs into flow cells at low flow to diminish the flow alignment of MTs on the coverslips. In our experiments, MTs were attached to coverslips via poly-L-lysine chains and the attachment was often very loose, with long MT segments free from surface constraints. This experimental setup allowed us to generate MT-MT junctions with a variety of angles (Fig. 1, *B* and *C*; Movies S2 and S3).

We found that, in agreement with in vivo data, cargo activity often deformed MTs at intersections, typically in a reversible fashion such that MTs returned to their original configuration upon cargo passage (Fig. 1, *B* and *C*). Cargos driven by high numbers of kinesin-1 motors (baseline concentration, marked by * in Fig. S1) dwelled for extended periods of time at MT intersections: 55.0% of events (60 of 109) lasted for more than 1 s. Outlier dwells as long as 60 s were observed (Fig. 2).

To examine whether the effect was due to a motor tug-of-war, we increased the effective motor number on the cargos using two strategies: 1) we incubated beads with a 10× higher motor concentration (** in Fig. S1), and 2) we used 10× diluted motility buffer (since kinesin's affinity for MTs depends on the overall salt concentration). In both cases, we observed an increase in the percentage of dwells longer than 1 s: 68.2% (58 of 85) for the 10× motor assay and 61.8% (63 of 102) for the low-ionic-strength assay. The mean dwell times increased for all angle ranges: the increases were significant for the 0–30° and 30–60° angle ranges, but marginally insignificant for the 60–90° range. In addition, nearly half of the dwells that were longer than 5 s in the 10× KIF5A and 0.1 salt assays were associated with MT bending (16 of 34 and 11 of 27, respectively). Our results are consistent with the hypothesis that motors at MT intersections undergo tug-of-war events, and that such competition can lead to exceedingly long cargo dwell times. The lack of or marginal change in dwell times across our assays for nearly normal intersections is consistent with theoretical prediction (11).

Most of the exceedingly long dwell times occurred for very acute junction angles. For example, in our baseline assay, all pauses longer than 50 s occurred for angles below 30°. Conversely, cargo dwell times for angles above 70° were all below 1 s. The dwell times for the crossings in the 60–90° range were significantly lower than those for the 0–30° range ($p < 1e\text{-}5$ for all assays).

For long pauses, the tracking records were often long enough for us to examine the dynamics at the intersection (Fig. 3). Cargo velocities during the time the cargos were associated with two MTs were variable. In some cases, noise made identification of segments of constant velocity ambiguous. However, even selecting only the clear segments of constant velocity still showed a dramatic slowdown, on average <300 nm/s in all assays discussed above (Fig. 3 *B*). Cargos were not slowing down due to high number of motors working together (12) or motor crowding (10,11), since motor velocities appeared healthy away from MT crossings (Fig. S2).

The fact that cargos were not precisely stationary suggests that the motors were not blocked by an obstacle on

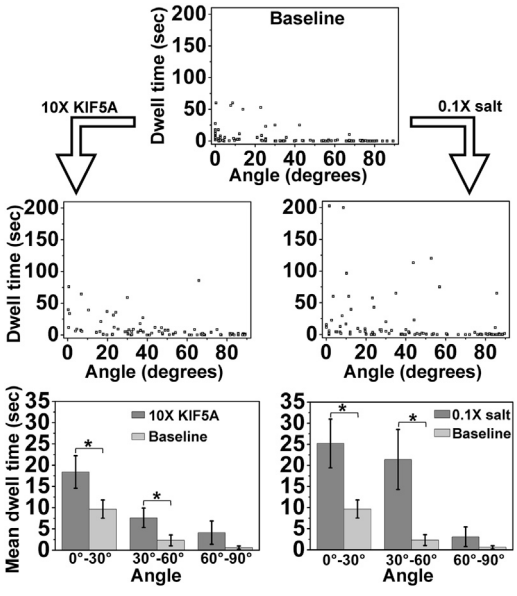

FIGURE 2 Effect of motor number on dwell times at MT intersections as a function of angles between undeformed MTs. Top: baseline assay ($n = 109$). Middle: assays with 10× motor number ($n = 83$) or low ionic strength ($n = 95$), as indicated by angled arrows. Bottom: comparison of mean dwell times in 30°-wide bins for top and middle panel data (error bars: mean ± SE). Significant increases are indicated by asterisks (left to right: $p = 0.0496$, 0.0088, 0.0044, 1.2e-4).

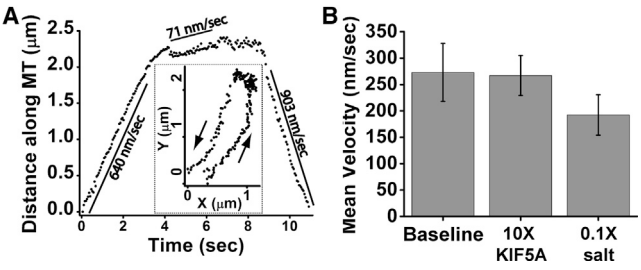

FIGURE 3 Long dwells consist of slow cargo motions. (*A*) Example of motion along nearly antiparallel MTs, projected along the MT direction. Healthy kinesin-1 motility is interrupted by a region of slow motion. Solid lines highlight select regions of nearly constant velocity (values shown). Inset: the actual track is shown. Arrows show the direction of cargo motion. (*B*) Bar graph of average velocities observed during dwells for assays in Fig. 2 as indicated.

MTs, so a tug-of-war is confirmed as the likeliest scenario. The velocities were low enough that they could not have arisen due to a plausible sideways load on the motors (15). Instead, the kinesin force-velocity relationship (15) suggests that individual motors had to experience at least 3.5 pN of backward load to match the observed slowdown. The actual slowdown was likely greater and the load per motor was even closer to stall because we excluded segments whose velocity was too low to extract from noise.

Why would a tug-of-war result in long dwell times? It is possible that geometry plays a direct role: a bead is in position to experience a tug-of-war so long as it overlaps both MTs (or is within motor length of both), so a nearly antiparallel layout of MTs could lead to longer dwell events. Our data do not rule this out, but its contribution is likely small. First, dwell events at an antiparallel MT geometry were often spatially localized (Fig. 3 *A*), suggesting that geometry is not the limiting factor for a tug-of-war. Furthermore, one can preferentially increase the bead-MT overlap for MT intersection angles close to 90° by using larger beads (the overlap for nearly aligned MTs is not limited by bead size). Experiments with 3 μm beads showed dwell times comparable to those observed with 1 μm beads (Fig. S3).

We propose that a more prominent contribution to long dwells may be made by extended kinesin-MT attachment times under high load (see Figs. S4 and S5 and Text S1 for further discussion) and reduced kinesin-MT attachment times under sideways load (12,13). The former could produce long dwells, while the latter could restrict long dwells to events with nearly antiparallel geometries. Further modeling in the future is needed to attain a quantitative description of the switching process.

CONCLUSIONS

In this study, we demonstrate that kinesin motors bound to cargoes can engage in an extended tug-of-war at MT intersections. Our data highlight the importance of factors that control the geometry of MT networks, and local regulators of the motor-MT affinity for MT-based transport. We also find that intersecting MTs that are not firmly fixed in space can be bent by passing cargos. Therefore, we propose that future efforts aimed at modeling cargo traversals of MT-MT crossings need to take into account MT deformations and the elastic properties of MTs rather than strictly focus on a fixed filament geometry.

Our finding that an increased number of motors on cargos leads to longer dwell events is consistent with the proposal that local agents that reduce motor-MT affinity can reduce or alleviate extended cargo pausing (1). Finally, our study also raises the question of how long-distance kinesin-driven transport occurs when antiparallel MT arrangements are present in cells (14).

SUPPORTING MATERIAL

Supporting Results and Discussion, five figures, and three movies are available at http://www.biophysj.org/biophysj/supplemental/S0006-3495(15)00181-2.

REFERENCES

1. Vershinin, M., B. C. Carter, …, S. P. Gross. 2007. Multiple-motor based transport and its regulation by Tau. *Proc. Natl. Acad. Sci. USA.* 104: 87–92.
2. Ross, J. L., H. Shuman, …, Y. E. Goldman. 2008. Kinesin and dynein-dynactin at intersecting microtubules: motor density affects dynein function. *Biophys. J.* 94:3115–3125.
3. Bálint, Š., I. Verdeny Vilanova, …, M. Lakadamyali. 2013. Correlative live-cell and superresolution microscopy reveals cargo transport dynamics at microtubule intersections. *Proc. Natl. Acad. Sci. USA.* 110:3375–3380.
4. Kosaka, S., H. Takuma, …, H. Mori. 2004. The distributions of tau short and long isoforms fused with EGFP in cultured cells. *Osaka City Med. J.* 50:19–27.
5. Tuma, M. C., A. Zill, …, V. Gelfand. 1998. Heterotrimeric kinesin II is the microtubule motor protein responsible for pigment dispersion in Xenopus melanophores. *J. Cell Biol.* 143:1547–1558.
6. Semenova, I., and V. Rodionov. 2007. Fluorescence microscopy of microtubules in cultured cells. *Methods Mol. Med.* 137:93–102.
7. Ikeda, K., I. Semenova, …, V. Rodionov. 2010. Melanophores for microtubule dynamics and motility assays. *Methods Cell Biol.* 97: 401–414.
8. Nascimento, A. A., J. T. Roland, and V. I. Gelfand. 2003. Pigment cells: a model for the study of organelle transport. *Annu. Rev. Cell Dev. Biol.* 19:469–491.
9. Smith, T. E., W. Hong, …, M. Vershinin. 2013. Single-molecule inhibition of human kinesin by adociasulfate-13 and -14 from the sponge Cladocroce aculeata. *Proc. Natl. Acad. Sci. USA.* 110:18880–18885.
10. Butterfield, J., W. Hong, L. Mershon, and M. Vershinin. 2013. Construction of a high resolution microscope with conventional and holographic optical trapping capabilities. *J. Vis. Exp.* http://dx.doi.org/10.3791/50481.
11. Erickson, R. P., S. P. Gross, and C. C. Yu. 2013. Filament-filament switching can be regulated by separation between filaments together with cargo motor number. *PLoS ONE.* 8:e54298.
12. Bieling, P., I. A. Telley, …, T. Surrey. 2008. Processive kinesins require loose mechanical coupling for efficient collective motility. *EMBO Rep.* 9:1121–1127.
13. Leduc, C., K. Padberg-Gehle, …, J. Howard. 2012. Molecular crowding creates traffic jams of kinesin motors on microtubules. *Proc. Natl. Acad. Sci. USA.* 109:6100–6105.
14. Conway, L., D. Wood, …, J. L. Ross. 2012. Motor transport of self-assembled cargos in crowded environments. *Proc. Natl. Acad. Sci. USA.* 109:20814–20819.
15. Block, S. M., C. L. Asbury, …, M. J. Lang. 2003. Probing the kinesin reaction cycle with a 2D optical force clamp. *Proc. Natl. Acad. Sci. USA.* 100:2351–2356.

Supplemental Material

Full title:

Cargo transport across microtubule intersections: evidence for prolonged tug of war between kinesin motors.

Running head:

Cargo transport across MT intersections

Olaolu Osunbayo*, Jacqualine Butterfield*, Jared Bergman*, Leslie Mershon*, Vladimir Rodionov[#], Michael Vershinin*[†]

* Department of Physics and Astronomy, University of Utah, Salt Lake City, Utah, 84112, USA

[†] Center for Cell and Genome Science, University of Utah, Salt Lake City, Utah, 84112, USA

[#] Department of Cell Biology, University of Connecticut, Farmington, Connecticut, 06030, USA

Fig. S1 Kinesin concentration reference curve. The binding fraction measurements for kinesin bead assays (∅1 μm) were well fit by a single motor curve (red). Motor incubation concentrations used in this study are shown by arrows and stars (* : 0.064 nM ; ** : 0.64 nM). Nominal motor to bead molar ratios were 850:1 and 8500:1 respectively. For comparison with previously published results, note that here kinesin concentration is shown on logarithmic scale.

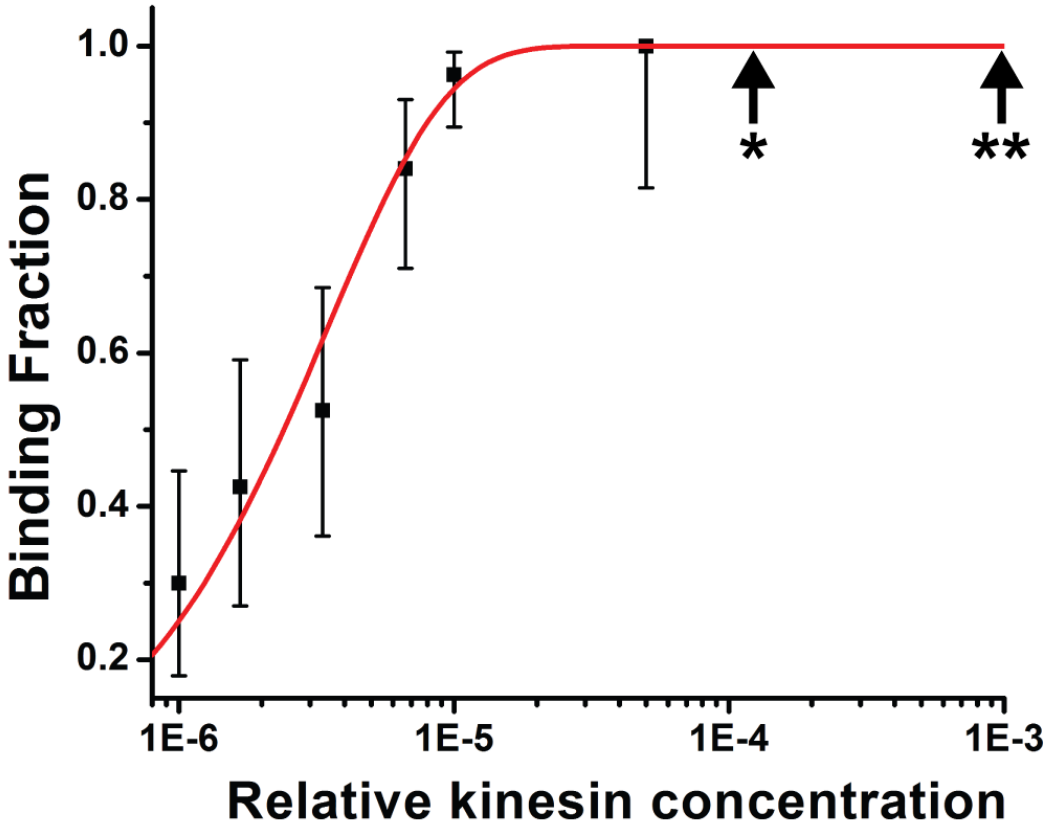

Fig. S2 Cargo velocity when moving along stand-alone MTs. Motor velocities were broadly peaked around 746 ± 51 nm/sec (mean ± SE).

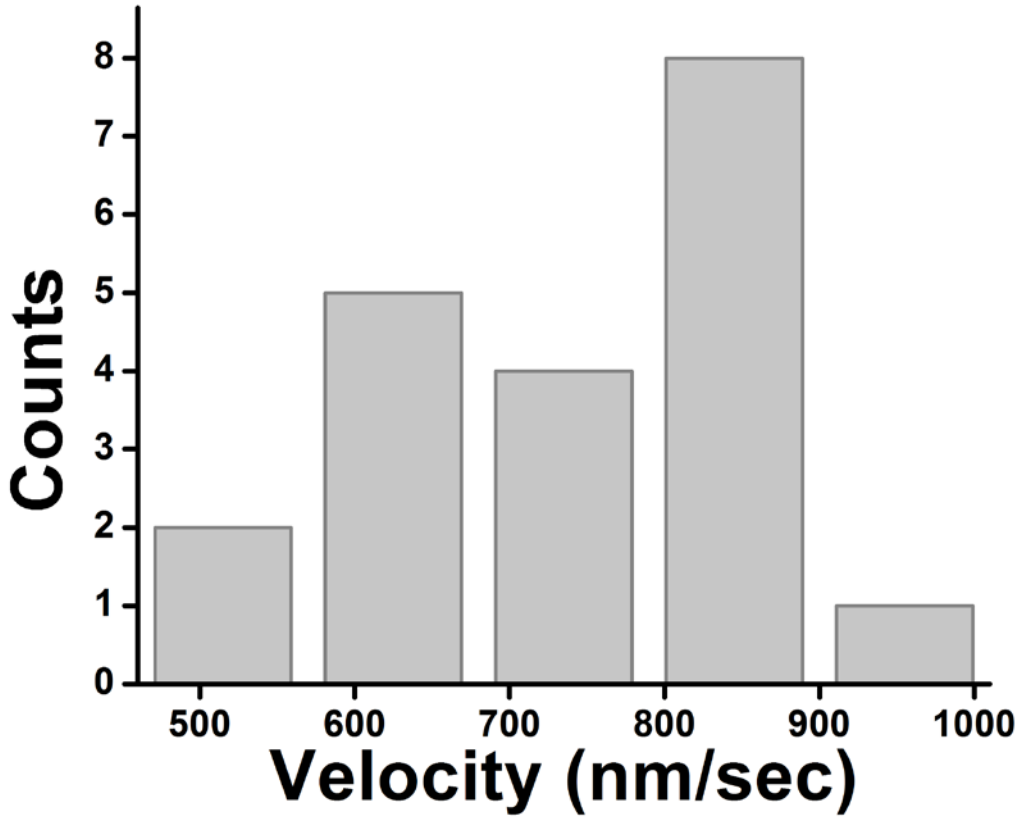

Fig. S3 The angular dependence of dwell times for different size beads. Bead assays for ∅1 μm and ∅3 μm beads were conducted to establish binding fraction curves and in each case an equivalent assay (** in Fig. S1) was used to quantify cargo dwell times ar MT intersections. High motor concentration was chosen to maximize the probability of motor engagement on both MTs during each crossing event and thereby to minimize the probability of undercounting the more localized tug-of-war events. The observed differences were not significant. We observed no evidence that higher bead-MT overlap at intersections (as would be the case for larger beads) leads to a more uniform distribution of dwell times.

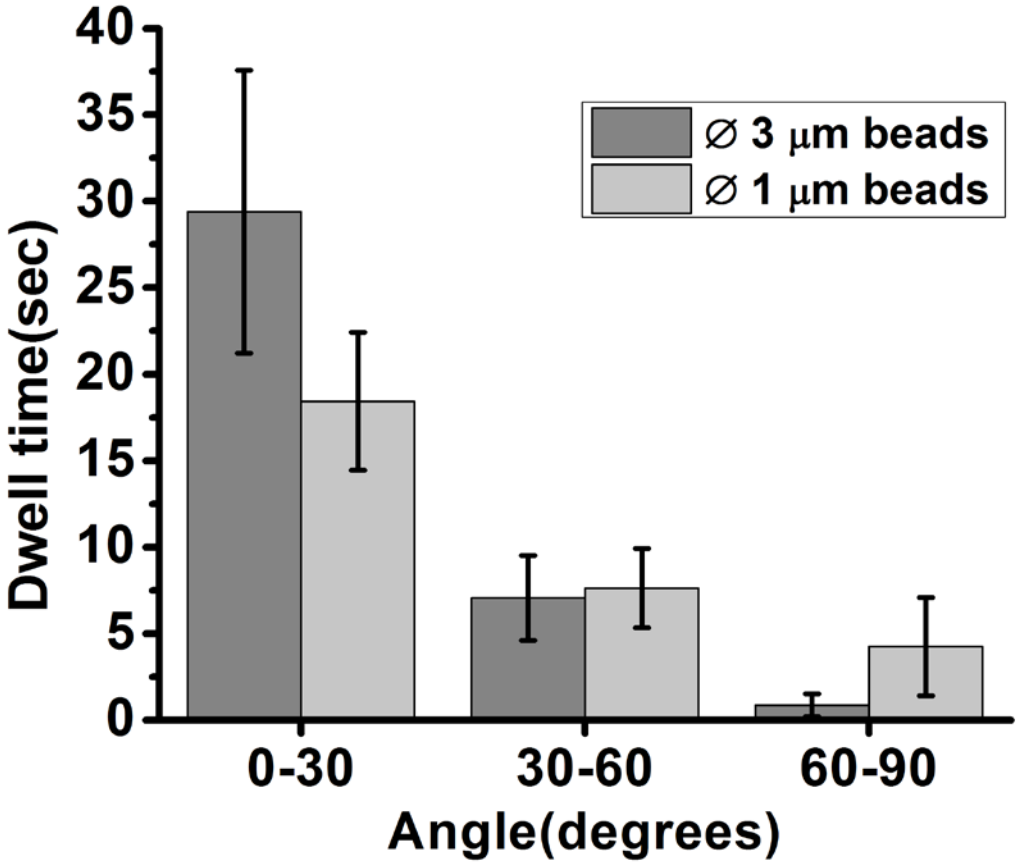

Fig. S4 The effect of MT-MT orientation on dwell times. Dwell times for cargos at intersections for baseline (left, n=59), high motor concentration (middle, n=44) and low salt concentration (right, n=40) assays are shown as a function of MT-MT angle. 180° angle corresponds to parallel MTs with identical polarity.

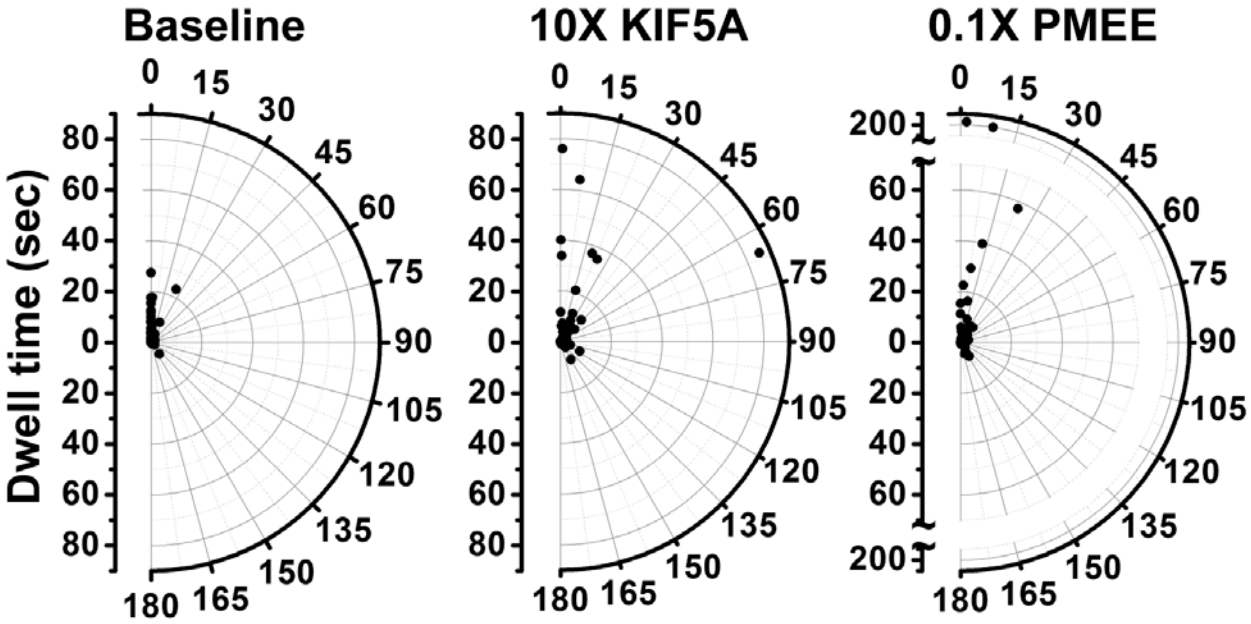

Fig. S5 Histograms of dwell times for intersections of MTs with known polarity. Dwell time distributions lower than 30 s are well fit by exponential decays (red lines) for the baseline, low salt, and high motor concentration assays. See Fig. S4 for angular distribution of these dwell times. Decays times extracted from fits are 3.2±0.4, 4.0±0.8, 5.3±0.4 s (left, middle, right panels respectively). Note that even though an exponential fit is a convenient way to characterize the decay of dwell time distributions, individual motor detachment times are likely to be less than 1 sec – far smaller than the bin size. Therefore it is not possible to tell whether the actual distribution is exponential or e.g. a higher order gamma distribution. We therefore cannot speculate whether single or multiple motor detachment events are associated with termination of dwells.

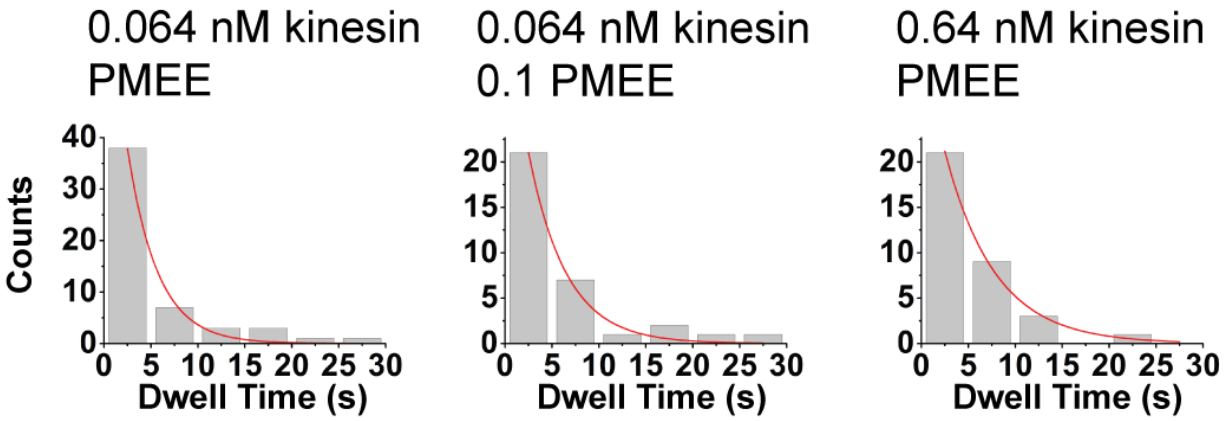

Supplemental Text S1

If cargo dwells at MT crossings are indeed due to opposing action of kinesin motors then one would expect this to occur preferentially for those acute intersection angles where MT polarity was opposite. We therefore attempted to segregate the latter acute angle crossings based on whether MT minus-plus directions were roughly aligned or roughly anti-aligned. We focused on a subset of MT crossings for which cargos switched filaments. In such cases, MT polarity could be inferred for both crossing filaments from the direction of cargo motion, and so the angles between positive directions of MT axes could be quantified.

The crossing angles for known MT polarity cases thus ranged between 0° and 180° rather than 0° to 90° for polarity-agnostic case (Fig. S4). The dwell times for MT crossing angles between 0° and 60° were significantly longer than for higher angles ($p = 0.039$ for baseline assay, $p<0.01$ for high motor and low salt assays). We further examined the 60°-120° range of crossing angles. All pausing events above 4 sec in duration for such crossings involved significant MT deformations. For example, the extreme outlier seen for high motor assay (Fig. S4, middle panel) corresponds to the case where MT crossing had an un-deformed angle of 65.9° but became completely anti-parallel due to cargo activity. The distribution of dwell times for all intersection angles pooled together in all cases was well approximated by an exponential decay (Fig. S5) with a few notable outliers. All outlier events occurred for crossings with nearly opposite MT polarities (0°-30° range), though in the special case discussed above the alignment resulted from MT bending rather than a priori geometry.

Legends to supplemental movies.

Supplemental Movie 1. Cargo motion across an intersection in vivo. Melanosome moving along fluorescently labeled MT in a melanophore encounters another MT, and this encounter leads to buckling of MT that serves as a transport track, and eventual pausing of the melanosome. Numbers indicate time in seconds. Magnification bar is 5 μm.

Supplement Movie 2. Cargo motion across an intersection *in vitro*. An example movie of a crossing event with substantial MT deformation during the crossing. This event corresponds to a sequence of frames shown in Fig. 1B Conformations of MTs before and after the event is comparable. Magnification bar is 2 μm.

Supplement Movie 3. Cargo motion across an intersection *in vitro*. An example movie of a crossing event with a long pause at the intersection during the crossing. This event corresponds to a sequence of frames shown in Fig. 1C. Magnification bar is 4 μm.